Energy-efficient Closed-loop Speed Control for 4WD Electric Vehicle E-motors During the Disconnect Clutch Transient Periods

Branimir Škugor* and Joško Deur
University of Zagreb, Faculty of Mechanical Engineering and Naval Architecture
e–mail: branimir.skugor@fsb.unizg.hr, josko.deur@fsb.unizg.hr

ABSTRACT

This paper deals with design of an energy-efficient e-motor speed control strategy, which is employed during e-motor connect and disconnect transients within electric vehicle powertrains with multiple e-motors and disconnect clutches. The proposed control strategy consists of open-loop feedforward control actions aimed to track energy-optimal speed and torque reference profiles, and a conventional speed feedback controller intended to enhance transient and steady-state control accuracy. The optimal feedforward control profiles are derived offline by using dynamic programming (DP) optimization and targeting different connect/disconnect motor speeds. The proposed control strategy is first evaluated through computer simulations against the conventional, time-optimal baseline feedback controller, where the emphasis is on evaluating the energy savings during the clutch connect and disconnect transients. The strategy is then incorporated into a previously developed optimal front/rear-axle torque vectoring control law and executed over different certification driving cycles, in order to assess the overall energy savings gained by energy-efficient e-motor connect/disconnect control.

KEYWORDS

Electric vehicles, multiple e-motors, disconnect clutches, torque vectoring, e-motor speed control, energy efficiency, dynamic programming.

INTRODUCTION

Electric vehicles (EV) with multiple e-motors exhibit actuator redundancy, which can be exploited by means of torque vectoring to reduce the energy consumption [1]. Equipping the e-motors with disconnect clutches introduces a room for additional energy savings due to avoidance of electromechanical drag of inactive electric motors [2, 3]. Prior to activating/connecting an inactive e-motor through locking corresponding dog clutch, the motor speed needs to be synchronized to the wheel speed referred to the motor shaft, which requires energy drawn from the battery. On the other hand, when disconnecting the e-motor, the related clutch is first opened which is followed by e-motor stopping in a regenerative braking mode, which recuperates energy back to the battery. It is required that each of these transients end up within a single sampling time step of the superimposed torque vectoring control strategy. A conventional approach of realizing e-motor synchronization/stopping control is to apply a proportional-integral (PI) speed controller tuned according to the symmetrical optimum, which yields well damped and fast transient responses [3-5]. However, such a time-optimal speed control solution provokes high-torque transients, which are typically unnecessarily fast and energy inefficient. To improve the energy efficiency, the transient speed response can be

* Corresponding author

extended towards the end of the torque vectoring sampling interval while properly shaping the motor speed/torque time profile [6].

The reference [6] designs the energy-efficient connect/disconnect transient control law based on offline e-motor torque instantaneous optimization for a wide range of speeds and stores the obtained results in an appropriate lookup table. During the online operation, the optimal e-motor torque is retrieved from the respective lookup table in dependence on the current/measured motor speed. Although this instantaneous optimization-based open-loop approach is optimal for torque vectoring sampling time of sufficient duration, it may fail to reach the target end speed for a reduced sampling time duration and may be sensitive to disturbances (e.g., varying friction torque).

To exploit the full potential of energy efficiency improvement, this paper employs an offline dynamic programming (DP)-based optimization of e-motor speed trajectory for synchronization and stopping tasks, and different synchronization and initial motor speeds, respectively. Unlike the instantaneous optimization-based approach, the dynamic programming method accounts for the inherently transient synchronization/stopping process, thus providing globally optimal control trajectories for both long and short torque vectoring sampling intervals. The globally optimal results are further used for establishing a realistic (online) energy-efficient e-motor speed control strategy, which consists of (i) feedforward control that sets the DP-optimal speed and torque time profiles and (ii) feedback control ensuring transient and steady-state accuracy against the disturbance. The proposed strategy is verified against the conventional, symmetrical optimum-based strategy in terms of energy consumption and transient response duration. Finally, the related optimal synchronization and recuperation energies, calculated and stored in the form of maps for a wide range of synchronization/initial speeds, are plugged into the overall front/rear-axle torque vectoring control system and simulated over different certification driving cycles with the goal to assess the energy consumption reduction potential in realistic driving conditions.

The remaining part of the paper is organized into five sections. Section 2 provides an EV powertrain model. Section 3 presents the offline control trajectory optimization problem and corresponding results. Section 4 proposes the online energy-optimal e-motor speed control strategy. The simulation results are given in Section 5, while concluding remarks are drawn in Section 6.

EV POWERTRAIN MODEL FOR SUPERIMPOSED TORQUE VECTORING

The considered four-wheel drive (4WD) EV powertrain configuration[1] is shown in Fig. 1a. Each e-motor (M/G) is connected to the corresponding wheel via a single-speed transmission with gear ratio h and a dog clutch represented by its binary state c_i, $i \in \{1, 2, 3, 4\}$ [3, 5] (equal e-motors case). The clutches enable disconnection of inactive e-motors, e.g., when operating in two-wheel drive (2WD) modes, to avoid drag loss.

A control-oriented backward-looking (BWD) modelling approach is utilized to derive respective powertrain model (see [5] including validation results with respect to more accurate forward-looking model). The total wheel torque demand $\tau_{w,t}$ is calculated based on the longitudinal vehicle dynamics equation:

[1] The methods presented are fully applicable in the more often/practical case of single front and rear motors connected to front and rear axle wheels via open differentials (a dual-motor powertrain).

$$\tau_{w,t} = \left(\left(m_v + m_{v,eq} \right) \dot{v}_v + m_v g \sin\alpha + R_o m_v g \cos\alpha + 0.5 \rho_{air} C_d A_f v_v^2 \right) r, \quad (1)$$

where m_v is the vehicle mass, v_v is the vehicle speed, g is the gravity acceleration, r is the effective tire radius, α is the road slope, R_o is the rolling resistance coefficient, ρ_{air} is the air density, C_d is the aerodynamic drag coefficient, A_f is the vehicle frontal area, and $m_{v,eq} = I_m h^2 / r^2 \sum_{i=1}^{4} c_i c_{R,i} + 4 I_w / r^2$ is the equivalent mass related to the motor I_m and wheel inertias I_w. The clutch state is denoted by a binary variable c_i, $i \in \{1, 2, 3, 4\}$, which takes the value of 0 if the respective clutch is open, and the value of 1, otherwise (i.e., for locked clutch). The clutch dynamics is described by the state equation:

$$c_i(k+1) = c_i(k) + c_{i,R}(k), \quad (2)$$

where $c_{i,R}$ represents a clutch state reference set by the torque vectoring strategy [3, 5]. Note that Eq. (2) incorporates one-step delay, meaning that a single sampling interval is deemed to be sufficient for the clutch to change its state from open to locked, and vice versa. In the case of clutch connect transient, i.e., when $c_i(k) = 0$ and $c_{i,R}(k) = 1$, the respective e-motor should first be started up (in idling conditions) to synchronize with the wheel speed referred to the motor shaft, after which the dog clutch is allowed to be locked. In the case of clutch disconnect, i.e., when $c_i(k) = 1$ and $c_{i,R}(k) = 0$, the dog clutch is first opened, and then the respective e-motor is stopped (again in idling conditions) by means of regenerative braking while recuperating energy back to the battery.

For the considered straight-line driving, only torque distribution among front and rear wheels determined by a dimensionless parameter σ is performed to satisfy $\tau_{w,t} = \sum_{i=1}^{4} \tau_{w,i}$:

$$\begin{aligned} \tau_{w,1} &= \tau_{w,2} = 0.5 \sigma \tau_{w,t}, \\ \tau_{w,3} &= \tau_{w,4} = 0.5 (1 - \sigma) \tau_{w,t}, \end{aligned} \quad (3)$$

where equal distribution among left and right wheels on both axles is assumed (optimal in the case of considered straight-line driving [4]). The torque vectoring control determining the torque distribution parameter σ is meant to be performed in a discrete-time manner, with a time discretization ΔT set to 1 s, herein.

The e-motor torques $\tau_{m,i}$ are calculated to cover the related wheel torques $\tau_{w,i}$, the transmission torque loss accounted for via torque-dependent efficiency η_{tr} (Fig. 1d), and the idle power loss P_0 (Fig. 1c):

$$\tau_{m,i} = \frac{1}{h} \left(\tau_{w,i} \eta_{tr}^{k_t}(\tau_{w,i}) + \frac{P_0(\omega_{w,i})}{\omega_{w,i}} \right), \quad (4)$$

where k_t takes value -1 for motoring case ($\tau_{w,i} > 0$) and 1 for regenerative braking case. The motor speed derives from the vehicle velocity v_v as

$$\omega_{m,i} = h \omega_{w,i} = h \frac{v_v}{r(1 - s_{x,i})}, \quad (5)$$

where $s_{x,i}$ is the longitudinal slip derived from the linearized tire model $s_{x,i} = \tau_{w,i} / \left(r k_x (F_{z,i}) \right)$ with k_x being the tire longitudinal stiffness and $F_{z,i}$ the acceleration-dependent normal load (for more details see [3, 5]).

The electric power of individual e-drive $P_{el,i}$ is calculated as

$$P_{el,i} = \tau_{m,i}\omega_{m,i} + P_{m,loss,i}\left(\omega_{m,i}, \tau_{m,i}\right), \tag{6a}$$

where $P_{m,loss,i}$ represents the e-drive power loss calculated from the efficiency map η_m (Fig. 1b) when the motor is enabled, and the power drag loss map P_d (Fig. 1c) when the motor is disabled (i.e., freely rotates):

$$P_{m,loss,i} = \begin{cases} \omega_{m,i}\tau_{m,i}\left(\eta_{m,i}^{\nu}\left(\left|\omega_{m,i}\right|, \left|\tau_{m,i}\right|\right) - 1\right), & \text{if } \tau_{m,i} \neq 0, \\ P_d\left(\left|\omega_{m,i}\right|\right), & \text{if } \tau_{m,i} = 0, \end{cases} \tag{6b}$$

The exponent ν equals -1 for motoring ($\tau_{m,i} \geq 0$) and 1 for regenerative braking ($\tau_{m,i} < 0$).

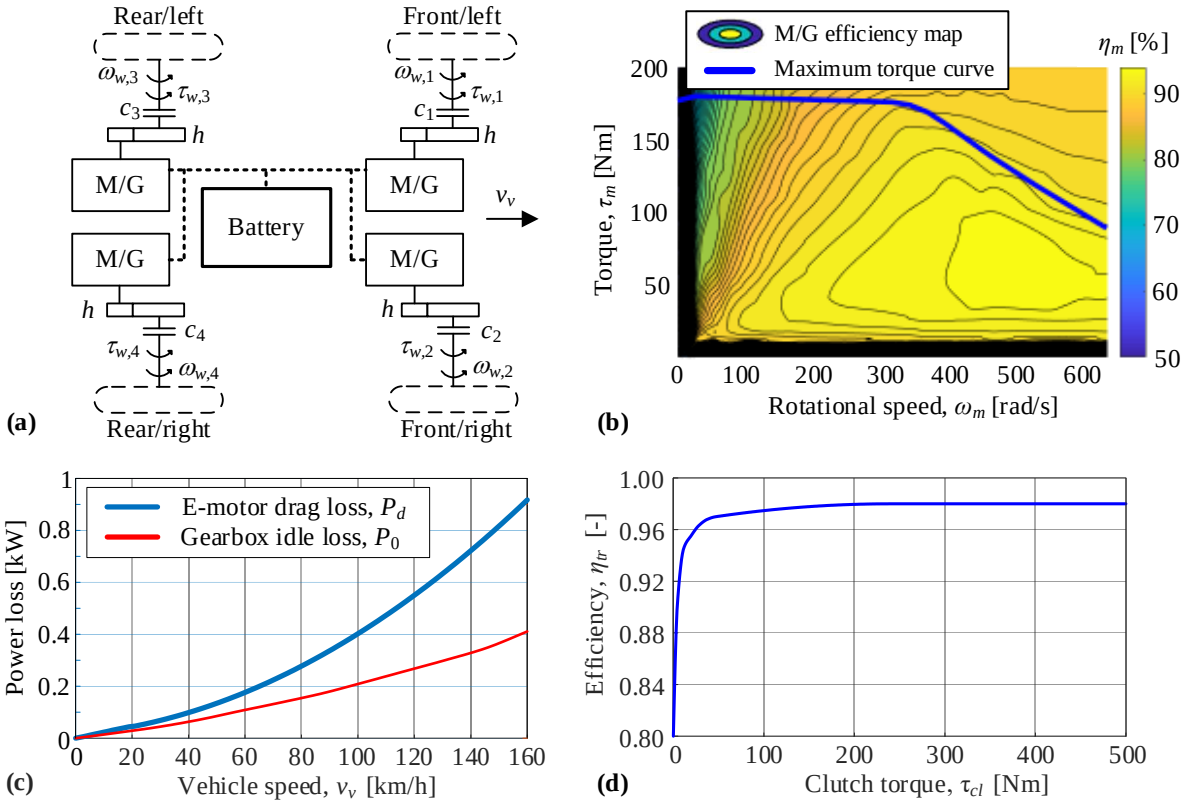

Figure 1. Schematic of 4WD EV powertrain configuration (a), M/G machine efficiency map (b), e-motor drag and gearbox idle power loss characteristics (c), and transmission efficiency (d)

CONTROL TRAJECTORY OPTIMISATION

This section deals with offline optimization of e-motor torque control trajectory (and, correspondingly, e-motor speed state trajectory) for clutch connect and disconnect transient intervals. As the method holds for each e-motor, the subscript *i* denoting individual e-motors is omitted from the variables for the sake of brevity.

Problem formulation

The cumulative energy loss is selected as a cost to be minimized

$$J = \sum_{k=0}^{N_f - 1} \left(P_{m,loss}\left(\omega_m(k), \tau_m(k)\right) + P_0\left(\omega_m(k)\right)\right)\Delta t, \tag{7}$$

where Δt is the e-motor speed control sampling time (set to 5 ms here), while $N_f = \Delta T/\Delta t$ is the total number of discrete time steps over the optimization horizon ΔT that corresponds to superimposed torque vectoring sampling time. As explained in the previous section, it is assumed that the e-motor speed transient during the connect and disconnect transients is finished within the superimposed control sampling interval ΔT. The power loss $P_{m,loss}$ is calculated according to expression (6b), while the idle power loss P_0 is given by the map shown in Fig. 1c. The motor torque variable τ_m is optimized as a control input (not calculated from the wheel torque based on Eq. (4) since the clutch is disconnected during the motor connect/disconnect transient intervals), while the motor speed variable ω_m is obtained from the motor rotational dynamics equation, as described below (not determined from the vehicle velocity, Eq. (5), as if the clutch were connected).

The e-motor rotational dynamics are described as

$$I_m \frac{d\omega_m}{dt} = \tau_m - \tau_0, \tag{8}$$

where τ_0 relates to the idle power loss P_0 as: $\tau_0 = \mathrm{sgn}(\omega_m) h\, P_0/\omega_m$ (see Eq. (4); sgn(.) is a signum function). The corresponding discrete-time state equation, after applying Euler discretization, reads:

$$\omega_m(k+1) = \omega_m(k) + \frac{\tau_m(k) - \tau_0(k)}{I_m}\Delta t. \tag{9}$$

The e-motor speed and torque variables are constrained within their lower and upper limits:

$$\omega_{m,\min} < \omega_m < \omega_{m,\max}, \tag{10}$$

$$-\tau_{m,\max}(|\omega_m|) < \tau_m < \tau_{m,\max}(|\omega_m|), \tag{11}$$

where $\omega_{m,\min}$ is set to 0 and $\omega_{m,\max}$ to 625 rad/s for the particular e-motor and control task (unidirectional motion), while the minimum and maximum torques are defined by speed-dependent maximum torque curve $\tau_{m,\max}$ shown in Fig. 1b. Note that the fast motor torque dynamics are neglected in optimization to reduce the computational complexity. Additionally, the e-motor speed is requested to end up (at the end of optimization horizon) in a predefined speed reference $\omega_{m,t}$:

$$\omega_m(N_f) = \omega_{m,t}, \tag{12}$$

which equals $\boldsymbol{h\omega_w}$ and 0 for the cases of motor connect and disconnect, respectively.

Optimization algorithm

The above optimization problem (7)-(12) is solved by using dynamic programming (DP) optimization algorithm, which gives globally optimal solutions for general non-convex and discontinuous optimization problems [7]. Since the DP algorithm requires amplitude discretization of state and control variables, the e-motor speed and torque variables are discretized with the resolutions of 5 rad/s and 5 Nm, respectively.

The DP optimization procedure first executes backward in time, by recursively minimizing (step-by-step) the following cost for each discretized speed value

$$J_j\left(\omega_{m,N_f-j}\right) = \min_{\tau_{m,N_f-j}} \left\{F\left(\omega_{m,N_f-j}, \tau_{m,N_f-j}\right) + J_{j-1}\left(\omega_{m,N_f-j+1}\right)\right\}. \tag{13}$$

where the sub-cost F represents the sub-integral cost from Eq. (7):

$$F = P_{m,loss}\left(\omega_{m,N_f-j}, \tau_{m,N_f-j}\right)\Delta t + P_0\left(\omega_{m,N_f-j}\right)\Delta t, \quad (14)$$

while J_{j-1} is the optimal cumulative cost function from the previous optimization step j−1. The speed in the following time step $N_f - j + 1$, i.e., ω_{m,N_f-j+1}, needed for deriving the cost J_{j-1}, is calculated from the state equation (9) based on the current speed ω_{m,N_f-j} and torque τ_{m,N_f-j}. If the speed ω_{m,N_f-j+1} falls in-between discretized grid values, a linear interpolation is used to get J_{j-1}. The initial cumulative cost for j = 0, i.e., i.e., for the final time step $k = N_f$ (see Eq. (12)), is obtained by penalizing the end speed deviation from the target speed:

$$J_0\left(\omega_{m,N_f}\right) = K_f\left|\omega_{m,N_f} - \omega_{m,t}\right|, \quad (15)$$

where the penalization factor is set to a relatively high value to enforce the final condition satisfaction (here set to $K_f = 10^8$). The speed and torque constraints (10) and (11) are strictly enforced by iterating only over allowed discretized values while minimizing (13).

The backward-in-time phase results in 2D maps of the optimal cumulative cost $J_{opt}(\omega_m, k)$ and torque $\tau_{m,opt}(\omega_m, k)$, which are used for reconstruction of the optimal speed and torque time profiles within the forward-in-time phase. The reconstruction procedure starts from the known initial state $\omega_m(0) = \omega_{m,i}$, set to 0 and $h\omega_w$ for the cases of motor connect and disconnect, respectively, and retrieves the optimal torque value for that speed from the backward phase-stored solution map $\tau_m(0) = \tau_{m,opt}(\omega_{m,i}, 0)$. This torque value is then fed to the state equation (9) to get the speed in the next time step $\omega_m(1)$. The retrieval of the optimal torque for speeds falling in-between grid discretized values is again overcome by means of linear interpolation. The procedure is repeated in the forward direction until the end of time horizon, thus resulting in the optimal profiles: $\tau_m(0), \tau_m(1), \ldots, \tau_m(N_f - 1)$, and $\omega_m(0), \omega_m(1), \ldots, \omega_m(N_f)$. The torque at the final step N_f is set to 0, $\tau_m(N_f) = 0$, to keep the achieved target speed.

Analysis of optimisation results for startup case

Firstly, the DP optimization is performed for the e-motor connect case, in which the e-motor is accelerated from the zero speed, $\omega_{m,i} = 0$, to a target speed $\omega_{m,t}$. Fig. 2 shows the DP results for the case of setting the target speed reference to the maximum value $\omega_{m,t} = 625$ rad/s, and for the case of omitted and included idle power/torque losses represented by P_0 and τ_0 in Eqs. (7) and (8), respectively. The optimization time horizon length is set to ΔT = 0.5 s resulting in N_f = 100 optimization time steps for the sampling time Δt = 5 ms. Note that for the selected horizon length ΔT = 0.5 s, the synchronization transients can be finished within this horizon time interval (see [3] and Fig. 2).

Figs. 2a and 2b show the optimal speed time profiles over the DP backward phase-obtained optimal cumulative cost and torque maps, respectively. Note that the blank region of Fig. 2a corresponds to non-feasible region, meaning that the target speed cannot be achieved for the particular system if the e-motor speed and remaining time combination falls in that region. This region reveals that the minimum time to achieve the maximum target speed is around 140 ms. Certain pure delay in the speed response can also be observed, which is present to achieve the target speed right at the end of horizon, thus leading to the minimal energy consumption (i.e., reaching and keeping the target speed earlier would induce additional consumption due to drag losses, which are higher at higher speed, Fig. 1c). For the case of transmission idle power loss included, this speed delay is more pronounced, which is to minimize additional idle/drag power loss). The optimal torque versus speed profiles given in Fig. 2d follow the optimal knee points of the efficiency map (maximum efficiency points for the given speed/power) if only the motor

power losses are concerned. This profile somewhat deviates (lifts) from the optimal efficiency map knees in the case of idle power loss included, which is because of aforementioned extended response delay induced to minimize that loss. The optimal torque profiles shown in Figs. 2c and 2d exhibit an initial single-step maximum-amplitude peak, which is apparently to initially accelerate the motor while avoiding the low-efficiency low-speed region. This torque peak may cause an undesired initial torque jerky with no notable improvement in energy efficiency. Thus, it may be suppressed by imposing a constraint on torque input derivative (i.e., difference).

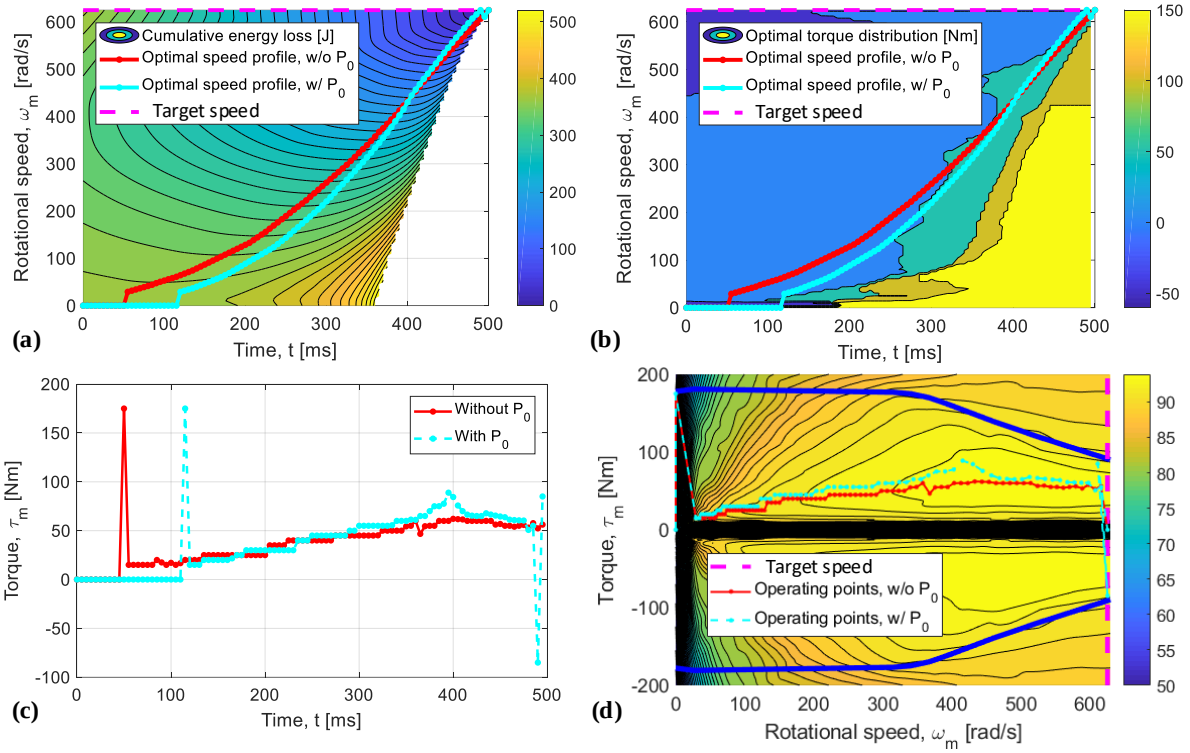

Figure 2. DP-optimal profiles of e-motor speed and torque for startup case ($\omega_{m,i} = 0\ rad/s$ and $\omega_{m,t} = 625\ rad/s$; w/ and w/o idle power loss P_0)

The optimal torque versus speed profile would deviate from the optimal efficiency knees even if the idle loss is omitted, provided that the startup time (i.e., the optimization horizon length ΔT) is short enough. This is demonstrated in Fig. 3 where the initial pure delay is set to 350 ms, leaving only 150 ms to finish the transient (note that these profiles can be reconstructed from the same DP backward phase-obtained maps given in Figs. 1a and 1b, i.e., new DP optimizations are not needed for the new initial conditions). As shown in Fig. 3b, the motor torque trajectory now gets closer to the maximum torque curve, i.e. it significantly deviates from the maximum-efficiency knee points, particularly at low motor speeds.

Deriving the cumulative cost function from the DP map (Fig. 2a) for different horizon lengths reveals the optimal trade-off between the total/cumulative energy loss consumption versus the transient duration (Fig. 4). These results show that the minimum time transient duration of 140 ms results in 43% higher energy loss when compared to the full-time transient duration of 0.5 s. The transient duration of 0.3 s, which is 40% reduction with respect to the full-time of 0.5 s, leads to only 3% higher energy loss, which may be considered as the appropriate/optimal trade-off (if there is a need for torque vectoring sampling time reduction to those levels, e.g., for faster torque response in sporty cars).

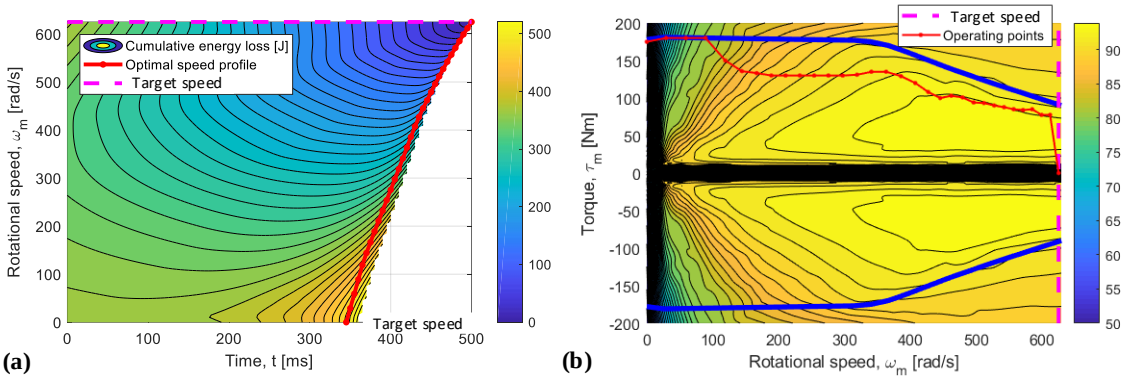

Figure 3. DP torque and speed profiles for shortened startup time (ΔT = 150 ms; $\omega_{m,i} = 0\ rad/s$, $\omega_{m,t} = 625\ rad/s$, no idle power loss P_0)

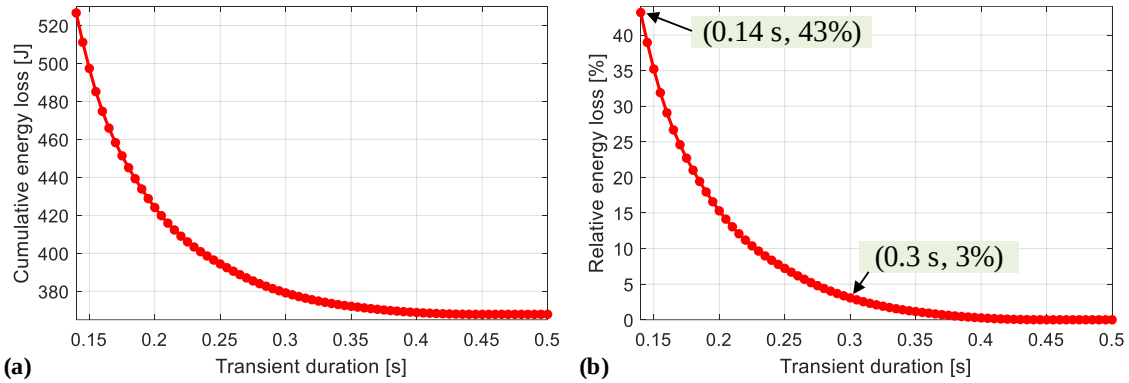

Figure 4. DP results for different values of startup time ΔT ($\omega_{m,i} = 0\ rad/s$, $\omega_{m,t} = 625\ rad/s$, no idle power loss P_0)

Analysis of optimisation results for stopping case

The DP optimization is also performed for the e-motor disconnect case, in which the e-motor is stopped from its initial speed $\omega_{m,i}$ set here to the maximum value of 625 rad/s to the zero speed, $\omega_{m,R}$ = 0. Fig. 5 reveal similar speed transient patterns to those observed in the startup case, i.e., the torque versus speed profiles again align with the optimal-efficiency knee points for the time horizon of sufficient length (cf. Fig. 2) and deviate (lift) from the knee points for the sufficiently shortened horizon length (Fig. 6, cf. Fig. 3). Fig. 7 reveals similar energy loss consumption versus transient duration trade-off as in the startup case (cf. Fig. 4).

Full set of results

Multiple DP optimizations are performed for e-motor startup and stopping cases and different target and initial speeds, respectively, in order to gain practical insights in support of e-motor speed control system design. Fig. 8 shows the results obtained in the case of omitting the idle power loss P_0 and setting the optimization time horizon of sufficient length (here ΔT = 0.5 s). These results point out that all the optimal torque versus speed profiles closely align with the knee point-related optimal efficiency line, i.e., they do not depend on the target or initial speed. Fig. 8c reveals that the initial pure delay of the startup-case response is the target speed-dependent in terms of being larger for smaller target speed. On the other hand, in the stopping case the initial time delay is zero, meaning that it is optimal to start braking immediately upon clutch opening to swiftly reduce the speed and corresponding drag loss. However, a delay-

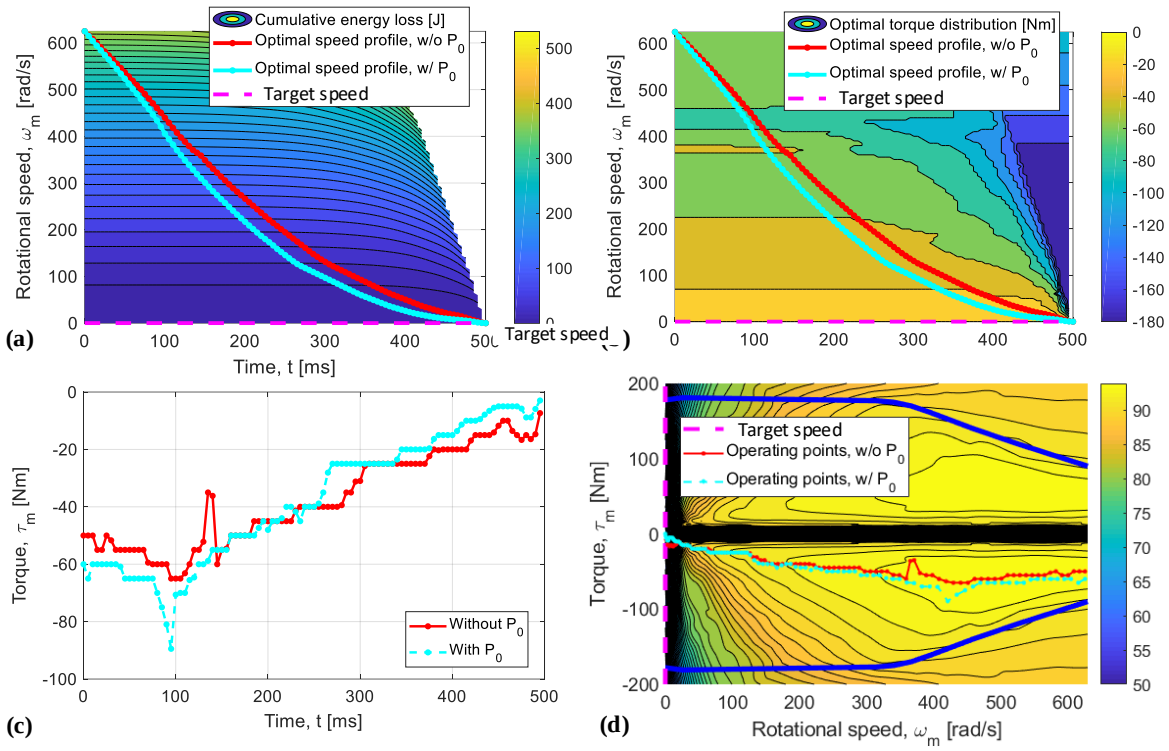

Figure 5. DP-optimal profiles of e-motor speed and torque for stopping case ($\omega_{m,i} = 625\ rad/s$ and $\omega_{m,R} = 0\ rad/s$; w/ and w/o idle power loss P_0)

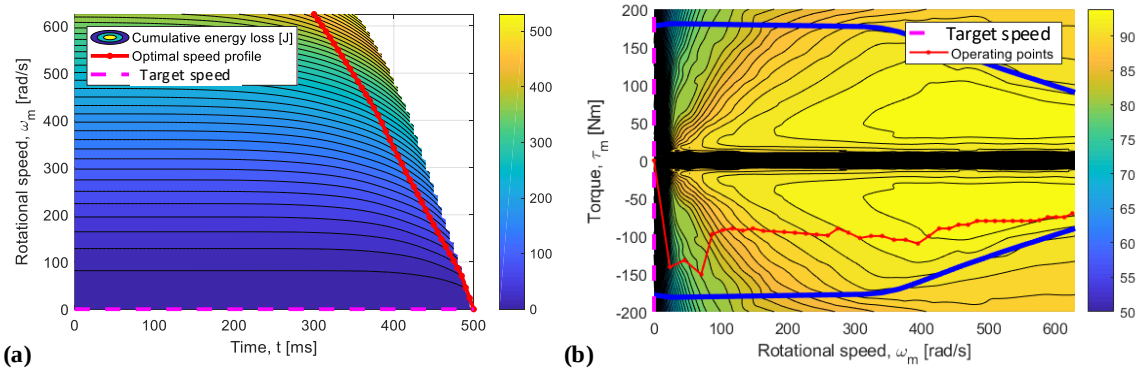

Figure 6. DP torque and speed profiles for shortened stopping time (ΔT = 200 ms; $\omega_{m,i} = 625\ rad/s$, $\omega_{m,t} = 0\ rad/s$, no idle power loss P_0)

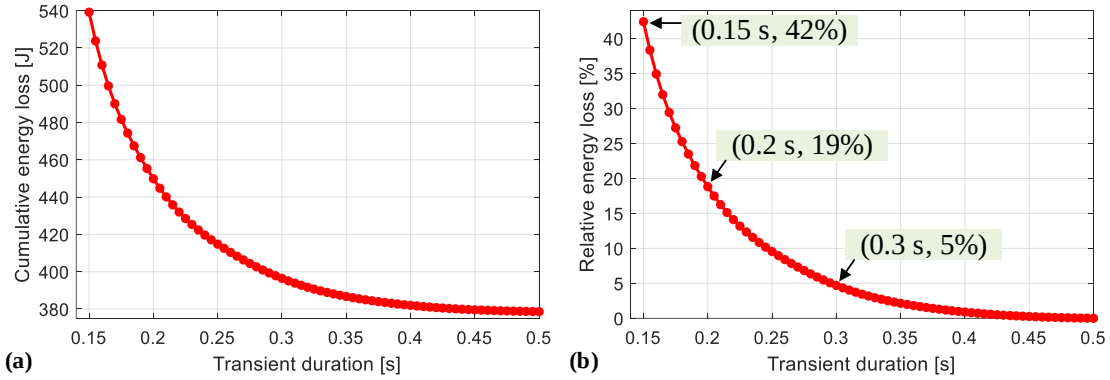

Figure 7. DP results for different values of stopping time ΔT ($\omega_{m,i} = 625\ rad/s$, $\omega_{m,t} = 0\ rad/s$, no idle power loss P_0)

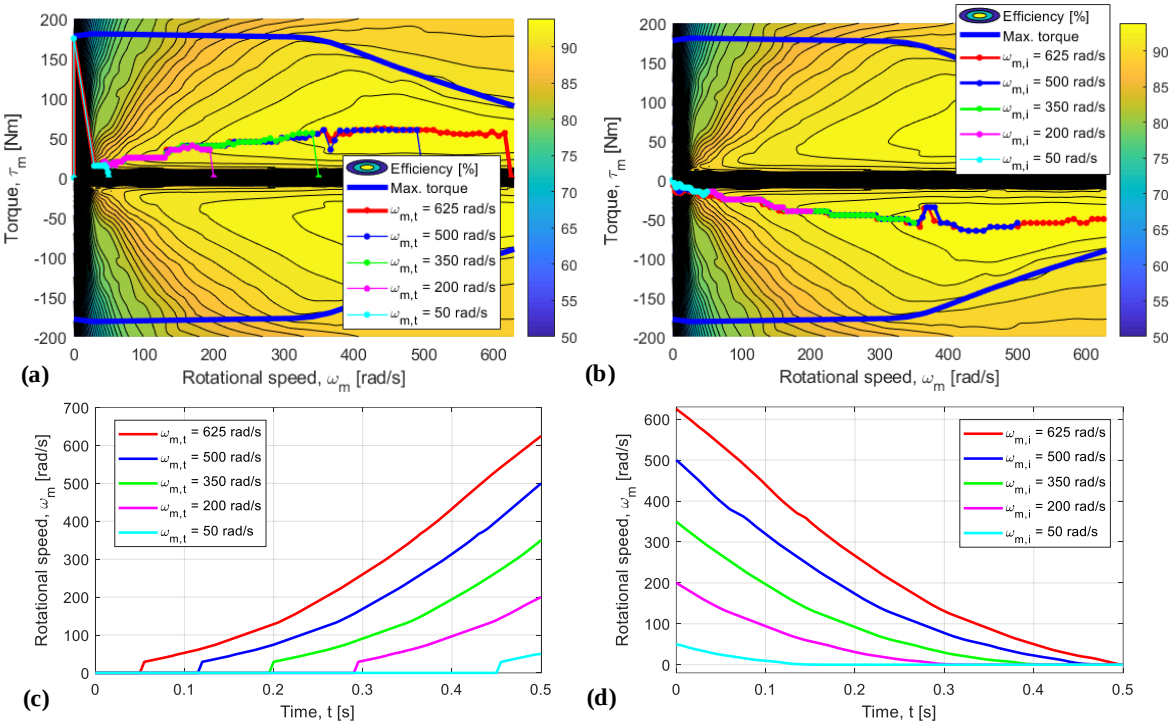

Figure 8. DP-optimal torque vs. speed profiles for different target speeds in startup/connect case (a), and different initial speeds in stopping/disconnect case (b) (ΔT = 0.5 s; idle loss P_0 not included)

drag loss is absent.

Fig. 9 shows the DP optimization results for the same scenarios and parameter setting as in Fig. 8, except for the optimization horizon being halved to ΔT = 0.25 s. Now, the time delay is reduced due to the smaller startup interval available, so that for larger target speeds the motor startup needs to start immediately (t_d = 0). The optimal torque versus speed profiles shown in Figs. 9a and 9b now deviate from the optimal efficiency line towards the higher-torque and lower-efficiency region, to reach the prescribed target speed within the reduced horizon. Moreover, those profiles are not aligned altogether unlike the case of ΔT = 0.5 s, because the profiles tend to approach the optimum efficiency line when possible (i.e., for lower speed targets) to improve the efficiency. The torque lift is more emphasized at lower speeds (a pulse-shape torque profile), which is apparently because the power loss excess with respect to minimal knee-point loss is smaller (in absolute sense) at lower velocities, i.e., lower powers (for roughly comparable efficiencies).

DESIGN OF E-MOTOR SPEED CONTROL SYSTEM

Time-optimal speed control

The baseline e-motor speed control system is based on a PI controller (Fig. 10), whose parameters are tuned according to the symmetrical optimum [8]:

$$K_R = 0.5\frac{I_m}{T_m}, T_R = 4T_m, \tag{16}$$

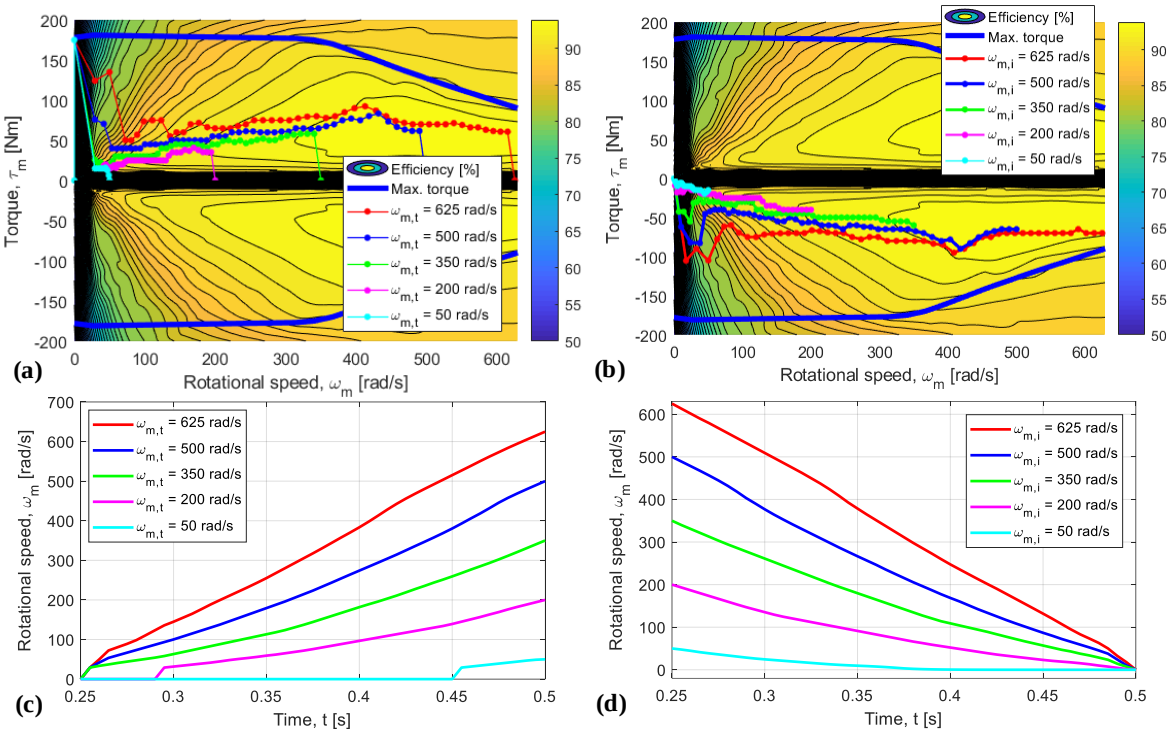

Figure 9. DP-optimal torque vs. speed profiles for different target speeds in startup/connect case (a), and different initial speeds in stopping/disconnect case (b) (ΔT = 0.25 s; idle loss P_0 not included)

where T_m represents the motor lag term model time constant (set to 10 ms). The PI controller is realized in a modified structure with the proportional term moved to the feedback control path, in order to avoid a high reference step speed overshoot. The controller output torque reference $\tau_{m,R}$ is saturated to satisfy the maximum torque curve limitation (see Fig. 1b). To account for the saturation, a hold on anti-windup intervention is introduced in the controller, which stops integration of the controller integrator whenever the controller output is saturated. The controller structured and parameterized in this way provides a fast quasi-aperiodic (well-damped) speed response with a relatively small overshoot (around 5%) in the small-signal operating mode, and a nearly minimum-time response in the large signal mode owing to swift activation of motor torque limit. Thus, the conventional speed control system in Fig. 10 may be considered as a (nearly) time-optimal one (for strict time optimality formulation and realization an interested reader is referred to [8]).

Energy-optimal speed control

The proposed energy-optimal speed control system is shown in Fig. 11. It consists of feedforward and feedback control paths. The feedforward path relies on the globally optimal DP results from the previous section, which are realized through maps of optimal motor speed and torque set in the speed and torque reference paths $\omega_{m,R,FF}$ and $\tau_{m,R,FF}$, respectively. In the

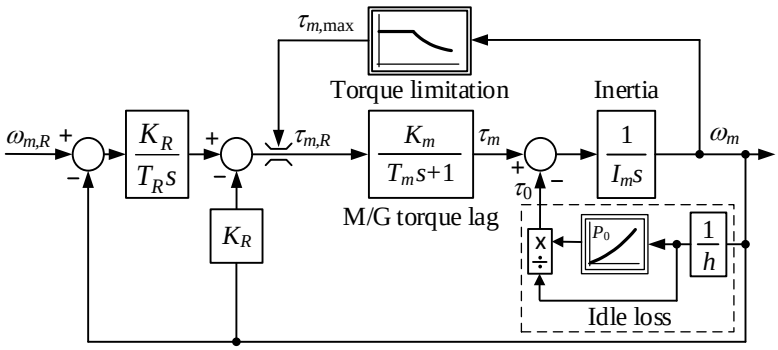

Figure 10. Block diagram of conventional, baseline e-motor speed control system ($\omega_{m,R}$ is equalized with target speed $\omega_{m,t}$)

general case, these are 3D maps depending on actual time, and the target speed $\omega_{m,t}$ in startup case or the initial speed $\omega_{m,i}$ in stopping case (see Fig. 9). Note that for the sake of simplicity of implementation the initial pure delay is not incorporated in the reference profiles for the startup case, i.e. it is replaced by the corresponding steady reference interval at the end of transient, resulting in certain suboptimality due to increased drag loss. Note also that the torque feedforward path sticks to zero when the target speed $\omega_{m,t}$ is reached (Fig. 11).

The torque feedforward path contributes to the speed of response, while the speed feedforward provides the tracking accuracy in the presence of unmodeled dynamics (e.g., the neglected motor lag in the optimized feedforward profiles). The speed reference tracking is again realized by the PI controller, which is again tuned according to the symmetrical optimum (see Eq. (16)). However, the PI controller is now given in standard rather than modified realization (with P term acting to the control error signal, cf. Figs. 11 and 10) to reduce the tracking error (note that the system in Fig. 11 operates in tracking mode, as opposed to system in Fig. 10 that runs in regulation mode).

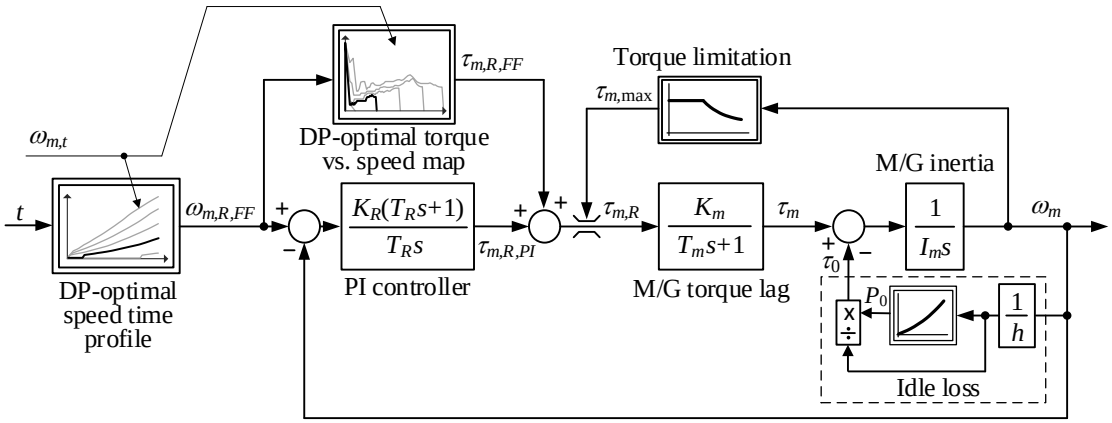

Figure 11. Block diagram of energy-optimal e-motor speed control system (applies to startup case).

In the alternative case of response settling (horizon) time ΔT being sufficiently high, the 3D feedforward maps reduce to 2D ones (see Fig. 8), which simplifies the control strategy implementation. Such implementation is considered herein, since for the concerned case $\Delta T = 0.5$ s the optimal maps are of 2D form (Fig. 8).

SIMULATION RESULTS

This section presents simulation results for the cases of e-motor startup (connect) and stopping (disconnect), as well as for the case of using the proposed e-motor speed controls within the superimposed EV powertrain torque vectoring control from [3, 5]. The full powertrain model, including idle power losses P_0, is used in simulations.

Startup case

Fig. 12 shows the e-motor speed and torque responses obtained by the time-optimal control strategy from Fig. 10 for the startup case and the speed target set to $\omega_{m,t}$ = 600 rad/s. The motor torque saturates to the maximum torque curve, thus providing a fast response (faster than required, Fig. 12a), which is compromised by the operation in suboptimal efficiency region (Fig. 12b). On the other hand, the energy-optimal speed control strategy (the simplified, 2D map-based version of that shown in Fig. 11) slows down the response to finish right in the required time ΔT = 0.5 s (Fig. 13a), while providing the operation in optimum-efficiency region (Fig. 13b). The accuracy of tracking the optimal speed and torque references is favourable, with certain errors observed only at low speeds and in the response settling period. The former is due to the high initial torque peak request, which cannot be instantly delivered due to the motor response lag (neglected in the offline optimizations). As discussed in the optimization section, this torque peak request can be reduced by adding a torque rate constraint in the optimization problem formulation. The latter is due to the instant deactivation of the feedforward action when approaching the speed target.

Table 1 lists the energy consumptions and settling time data related to results from Figs. 12 and 13. The total energy consumption $E_{el,t}$ is reduced by around 10% in the energy-optimal control case when compared to time-optimal control. This improvement is closely related to prolonged response settling time t_r (from 141 ms to 460 ms), which still satisfies the requested settling time ΔT = 0.5 s. The reduction of electric losses $E_{el,loss}$ is even more pronounced, i.e., they are nearly 40% lower in the case of energy-optimal control.

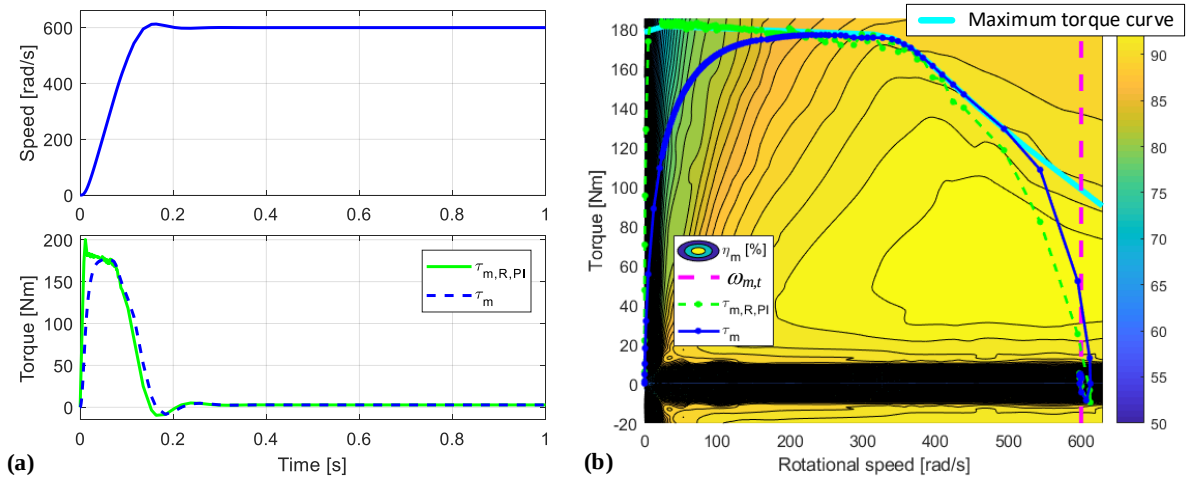

Figure 12. Speed and torque time responses for time-optimal speed control, startup case and target speed $\omega_{m,t}$ = 600 rad/s

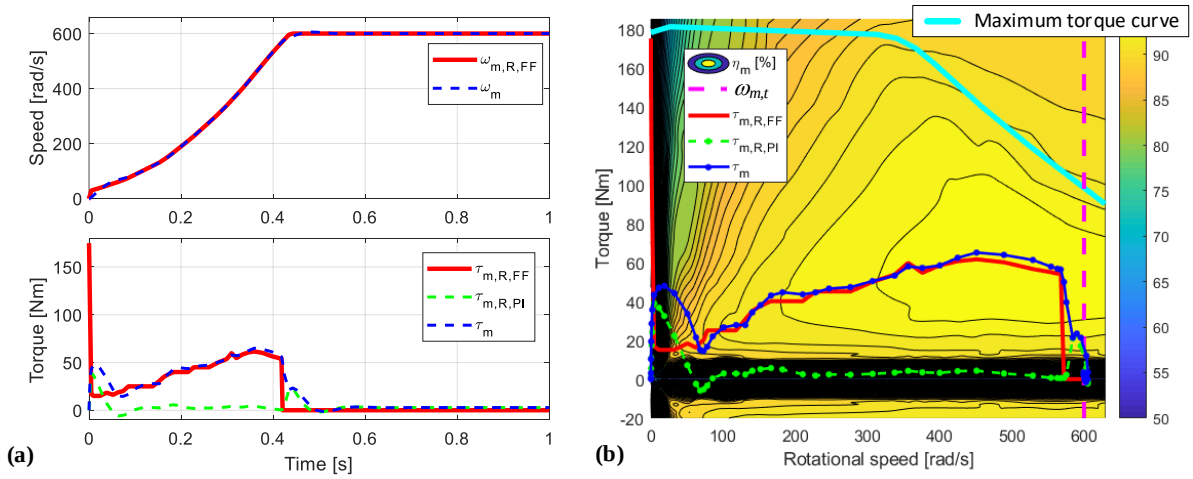

Figure 13. Speed and torque time responses for energy-optimal speed control, startup case and target speed $\omega_{m,t}$ = 600 rad/s

Table 1. Comparative performance indices of energy-optimal versus time-optimal motor speed control for startup case

$\omega_{m,t}$ = 600 rad/s	**Time-optimal**	**Energy-optimal**
$E_{el,loss}$ [J]	1271.3 (0.0%)	778.4 (−38.8%)
$E_{el,t}$ [J]	8237.7 (0.0%)	7383.5 (−10.4%)
t_r [ms]	141 (0.0%)	460 (+226.2%)

Stopping case

The stopping responses of the two control systems are shown in Figs. 14 and 15 for the initial speed $\omega_{m,i}$ = 600 rad/s. The corresponding performance indices are shown in Table 2. Again, the energy-efficient control strategy slows down the response towards the specified stopping time of 0.5 s, while maximizing the efficiency. This results in around 40% lower electric losses when compared with time-optimal control case (comparable to that of startup case, cf. Table 1), while recuperating 1.6% more energy to the battery by means of regenerative braking.

Full set of startup and stopping results

The comparative performance indices plots for full range of target speeds are shown in Figs. 16, 17 and 18. In the startup case, the application of energy-optimal control reduces the electric energy losses and the total energy consumption when compared to the time-optimal control by around 35% and 10%, respectively, in a wide range of target speeds (above 250 rad/s; Fig. 16). The results are generally comparable in the stopping case (Fig. 17), but with somewhat higher loss reduction (up to 60%) and lower recuperated energy gains, and opposite trends (higher gains at lower speeds). The response settling time is small along the whole target speed span, with the tendency to increase for high target/initial speeds (Fig. 18). On the other hands, the settling time reduces with the target/initial speed in the case of energy-optimal strategy, since the optimal torque path from Fig. 8 becomes shorter for smaller speed target. The remaining time to the full interval ΔT = 0.5 s corresponds to the idling interval (see Fig. 13).

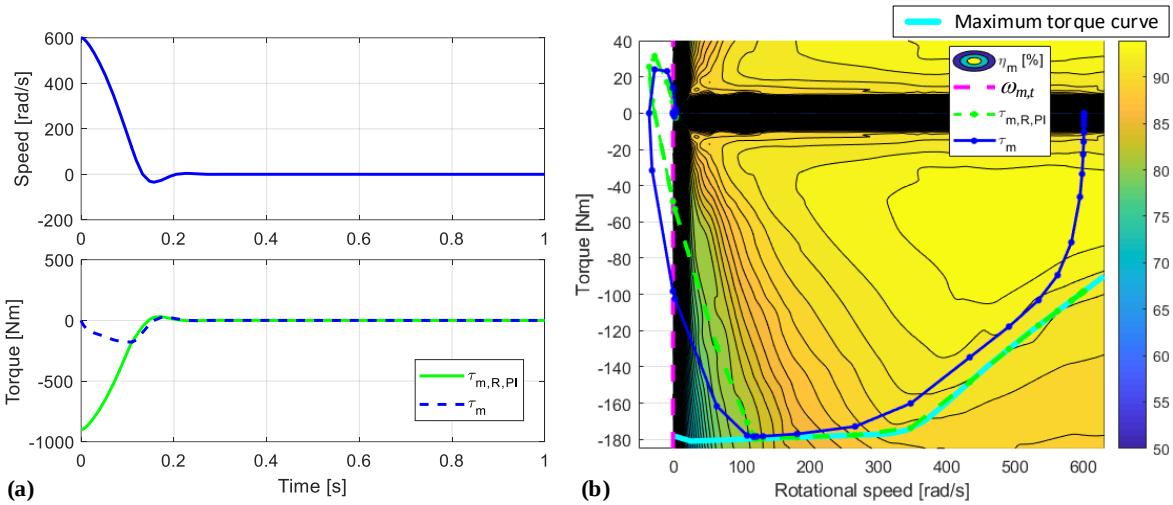

Figure 14. Speed and torque time responses for time-optimal speed control, stopping case and initial speed $\omega_{m,i}$ = 600 rad/s

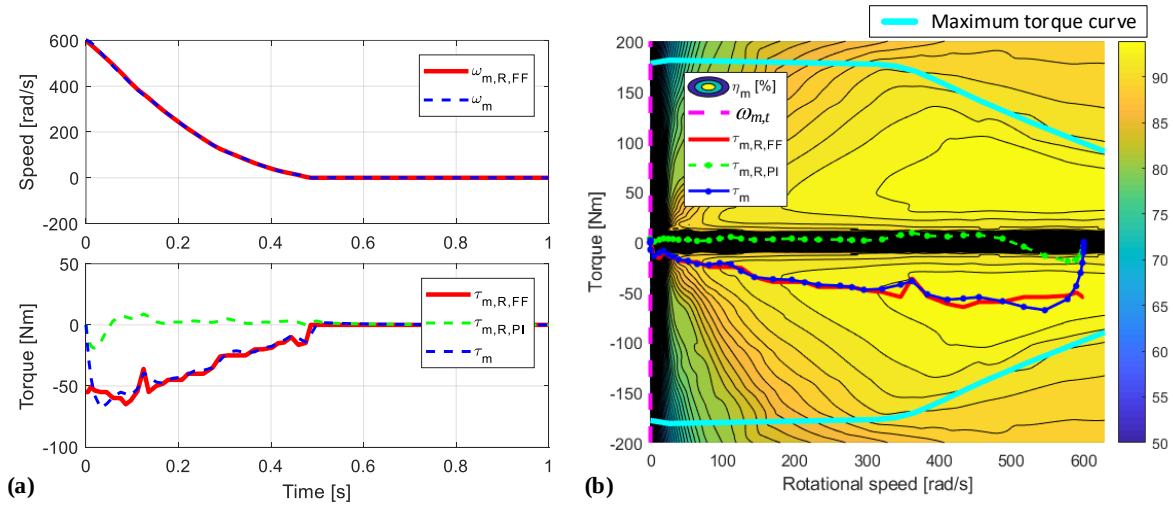

Figure 15. Speed and torque time responses for energy-optimal speed control, stopping case and initial speed $\omega_{m,i}$= 600 rad/s

Table 2. Comparative performance indices of energy-optimal versus time-optimal motor speed control for stopping case

$\omega_{m,i}$ = 600 rad/s	**Time-optimal**	**Energy-optimal**
$E_{el,loss}$ [J]	547.0 (0.0%)	332.4 (−39.2%)
$E_{el,t}$ [J]	−4738.2 (0.0%)	−4813.5 (+1.6%)
t_r [ms]	133 (0.0%)	486 (265.4%)

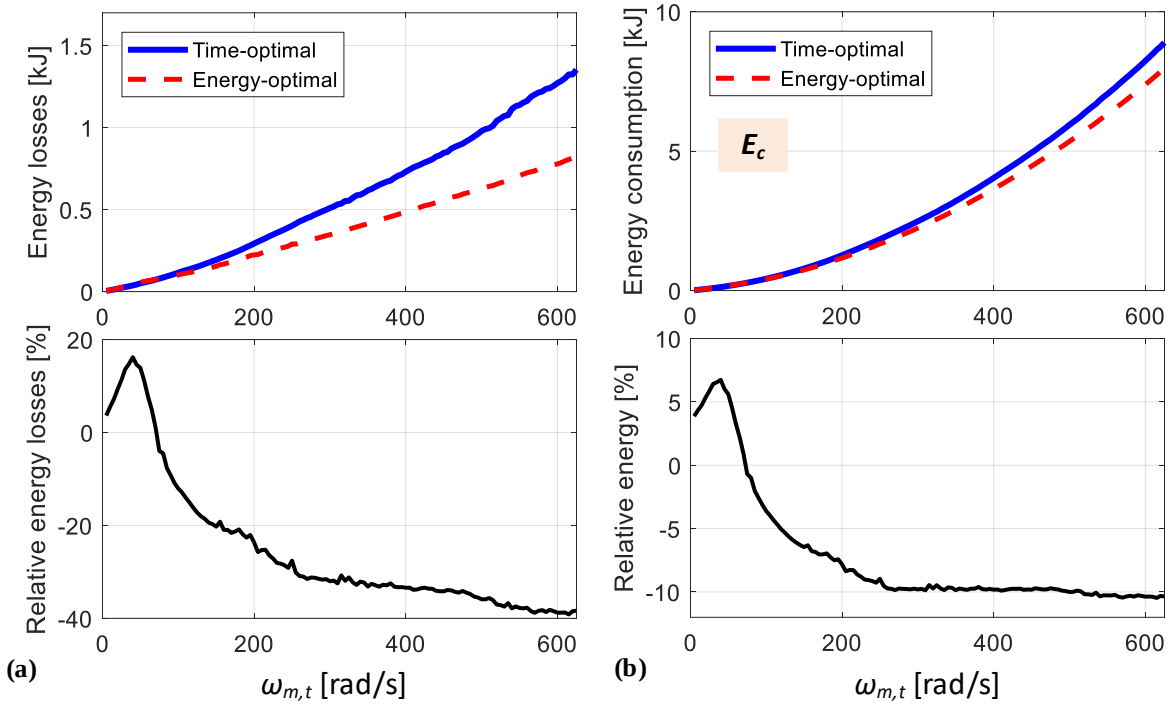

Figure 16. Energy loss and energy consumption indices for startup case, time-optimal and energy-optimal control strategies, and wide range of target speeds

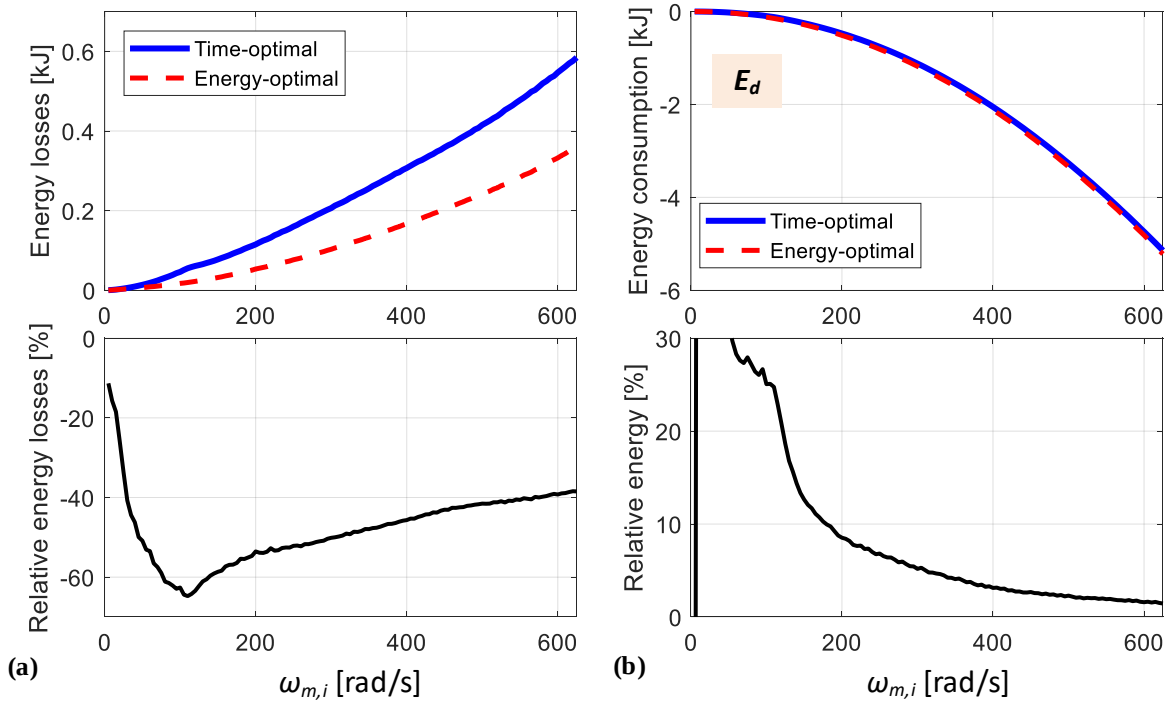

Figure 17. Energy loss and energy consumption indices for stopping case, time-optimal and energy-optimal control strategies, and wide range of initial speeds

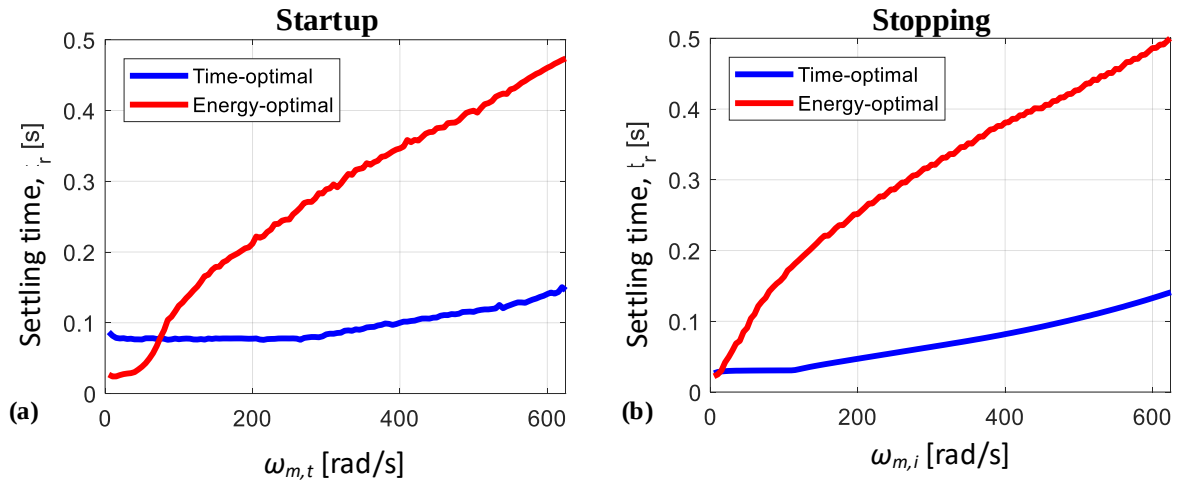

Figure 18. Comparative settling time plots for time-optimal and energy-optimal speed control systems, startup and stopping case, and wide range of target/initial speeds

Overall torque vectoring results

The above results corresponded to the intervals of e-motor startup and stopping idling intervals only, i.e., they relate exclusively to those sampling intervals in which the clutch changes its state. To test the proposed energy-optimal e-motor speed control strategy for the full vehicle (all motors) and the complete driving cycling (including the energy transfer to the wheels), the overall rule-based (RB) torque vectoring control system [3, 5] is executed over an updated backward-looking vehicle model. The update relates to replacement of target/initial speed-dependent connect (E_c) and disconnect transient energy consumption curves (E_d) given in [3, 5] for the conventional, time-optimal speed control strategy with those shown in Figs. 16 and 17 for the energy-optimal control strategy. The RB control strategy is set up for a favourable trade-off between minimization of energy consumption and number of clutch state changes [5].

Tables 3 and 4 show different energy loss and consumption indices corresponding to different certification driving cycles considered and time-optimal and energy-optimal speed control strategies, respectively. Expectedly, the energy-optimal control provides significantly lower electric losses than time-optimal control when only the connect and disconnect transient intervals are considered. The loss reduction is between 20 and 30% for startup/connect case and around 50% for stopping/disconnect case (see the first two rows of Table 4 and compare the

Table 3. Energy loss and consumption indices obtained by torque vectoring system simulation for time-optimal e-motor speed control strategy and different driving cycles

Cumulative energy consumptions [J]	**Driving cycle**				
	WLTP	**UDDS**	**US06**	**HWFET**	**NEDC**
$E_{el,loss,d,t}$	4480.1	2311.8	4491.2	900.6	1125.4
$E_{el,loss,c,t}$	8538.1	4483.2	9628.5	2348.9	1907.5
$E_{el,d,t}$	−19990.9	−9572.2	−27152.7	−4171.0	−4553.2
$E_{el,c,t}$	36614.2	18699.5	49059.4	10780.9	7765.3
$E_{el,t}$	11144758.1	4724681.4	7809487.7	7338298.0	4545033.0

$E_{el,loss,d,t}$, $E_{el,d,t}$ – electric losses and energy consumption over all disconnect steps,
$E_{el,loss,c,t}$, $E_{el,c,t}$ – electric losses and energy consumption over all connect steps,
$E_{el,t}$ – overall energy consumption during whole simulation.

results in Figs. 16 and 17). The corresponding connect-case energy consumption and disconnect-case recuperated energy (see third and four row of Table 4) is reduced in the former case and boosted in the latter case by around 8%. Although these savings are significant, the energy savings in terms of the total energy consumption all over the driving cycle (the last row of Table 4) are very small, i.e., below 0.1%. This is because the connection/disconnection energy represent only a small fraction of the total energy consumption. This may be explained by a relatively small number of clutch state changes and thus a small share of e-motor connect and disconnect intervals (see Table 5).

Table 4. Energy loss and consumption indices obtained by torque vectoring system simulation for energy-optimal e-motor speed control strategy and different driving cycles (percentages values within brackets are given with respect to values shown in Table 3)

Cumulative energy consumptions [J]	**Driving cycle**				
	WLTP	**UDDS**	**US06**	**HWFET**	**NEDC**
$E_{el,loss,d,t}$	2100.2 (−53.1%)	1057.3 (−54.3%)	2342.9 (−47.8%)	426.3 (−52.7%)	514.1 (−54.3%)
$E_{el,loss,c,t}$	6549.3 (−23.3%)	3539.3 (−21.1%)	6661.9 (−30.8)	1668.1 (−29.0%)	1516.5 (−20.5%)
$E_{el,d,t}$	−21484.4 (+7.5%)	−10387.7 (+8.5%)	−28296.2 (+4.2%)	−4464.3 (+7.0%)	−4948.9 (+8.7%)
$E_{el,c,t}$	33824.8 (−7.6%)	17409.0 (−6.9%)	44445.8 (−9.4%)	9786.9 (−9.2%)	7253.0 (−6.6%)
$E_{el,t}$	11140475.2 (−0.038%)	4722575.5 (−0.045%)	7803730.7 (−0.074%)	7337010.8 (−0.018%)	4544124.9 (−0.020%)

Table 5. Number of clutch state changes for simulations from Tables 3 and 4 (numbers in brackets represent total number of time steps within driving cycle)

WLTP	UDDS	US06	HWFET	NEDC
34 (1801)	20 (1370)	20 (601)	6 (766)	10 (1184)

The analysis is extended for the alternative RB control strategy parameterization, connected with the minimum energy consumption and maximum number of clutch state changes (see [5] and the last row of Table 6 in comparison with Table 5). The results shown in Table 6 indicate that the energy savings are now higher than in the nominal RB strategy tuning (cf. Table 4). Although they are still minor (up to 0.15%), it is worthwhile to use the proposed energy-optimal

Table 6. Total energy consumption and number of clutch state changes obtained by two e-motor speed control strategies and different driving cycles in case of RB torque vectoring strategy tuned for minimum energy consumption

	Driving cycle				
	WLTP	**UDDS**	**US06**	**HWFET**	**NEDC**
Time-optimal speed control, $E_{el,t}$ [J]	11126604.7 (0.0%)	4680147.6 (0.0%)	7814954.7 (0.0%)	7334062.0 (0.0%)	4521234.4 (0.0%)
Energy-optimal speed control, $E_{el,t}$ [J]	11118748.1 (−0.071%)	4673571.2 (−0.141%)	7807778.3 (−0.092%)	7332789.6 (−0.017%)	4519624.5 (−0.036%)
No. clutch state changes	136	88	32	6	36

motor speed control strategy, as it only relates to control software upgrade, provides reduced motor mechanical and thermal stress, and is not subject of disadvantages. Also, the energy consumption savings can be more significant for other model/vehicle parameters, particularly if the motor inertia is higher requiring more energy to start up/stop the motor (e.g., for e-trucks).

CONCLUSION

The paper has proposed an energy-optimal e-motor speed control strategy aimed at minimizing the energy consumption during connecting/startup and disconnecting/stopping events in electric vehicle (EV) powertrains with multiple e-motors and disconnect clutches. The control strategy was set to rely on globally optimal, offline-derived dynamic programming (DP) optimized e-motor torque and speed profiles implemented into the online feedback control strategy via feedforward actions.

When compared to the conventional, time-optimal baseline control strategy based on the PI controller tuned according to the symmetrical optimum criterion, the proposed energy-optimal control brings significant electric energy loss reduction in the e-motor connect and disconnect intervals (up to 40% for startup and 60% for stopping task). In terms of total energy consumption, the energy-optimal control provides up to 10% of savings. The energy-optimal response is slowed down compared with the time-optimal response to exhibit the torque vs. speed trajectory that follows the maximum efficiency (knee) points of the motor efficiency map. The response includes the zero-speed/zero-loss pause at the beginning of startup and end of stopping interval, so that the overall response settling time aligns with the required time interval corresponding to the superimposed torque vectoring strategy sampling time. If the required interval is short enough, the optimal torque trajectories lift above the maximum-efficiency line to complete the response timely, which is particularly emphasized in the low speed region where the share of absolute losses is relatively small. Although these energy savings were significant when considering the isolated connect and disconnect transients, they become quite small (up to 0.15%) when incorporating the energy-optimal controller into the overall torque vectoring strategy and executing it over a driving cycle. Nevertheless, it is still worth exploiting the energy-optimal strategy since it requires only a motor control software upgrade, reduce the motor mechanical and thermal stress, does not compromise any other implementation aspects, and may bring stronger energy efficiency benefits for other electric vehicle models, e.g., those related to electric trucks.

The future work could be directed towards a systematic analysis of influence of model parameters (e.g., the motor inertia and required response time) on the overall energy consumption, and implementation of a more general energy-efficient speed control strategy satisfying the requirement on short response interval (e.g. for sporty cars characterized by a short torque vectoring sampling time).

REFERENCES

1. S. Koehler, A. Viehl, O. Bringmann, and W. Rosenstiel, “Energy-Efficiency Optimization of Torque Vectoring Control for Battery Electric Vehicles”, *IEEE Intelligent Transportation Systems Magazine*, Vol. 9, No. 3, pp. 59-74, 2017.
2. Yang, S., Shin, B., Woo, M., Ahn, J. et al., “Disconnect Actuator System (DAS) for AWD EV’s Driving System,” SAE Technical Paper 2023-01-0451, 2023, doi:10.4271/2023-01-0451.
3. J. Deur, B. Škugor, W. Chen, Y. Zhang, E. Dai, “Energy-efficient Straight-line Driving Torque Vectoring for Electric Vehicles with Multiple Motors Equipped with Disconnect

Clutches", 18th Conference on Sustainable Development of Energy, Water, and Environment Systems (SDEWES), pp. 1-15, Dubrovnik, Croatia, Sep. 2023. (link)

4. B. Škugor, J. Deur, W. Chen, Y. Zhang, E. Dai, "Optimization of Straight-line Driving Torque Vectoring for Energy-efficient Operation of Electric Vehicles with Multiple Motors and Disconnect Clutches", *Optimization and Engineering*, 2024., https://doi.org/10.1007/s11081-024-09902-7
5. B. Škugor, J. Deur, W. Chen, Y. Zhang, E. Dai, "A Parameter-optimized Rule-based Control Strategy for Front-rear Torque Vectoring in Electric Vehicles with Multiple Motors and Disconnect Clutches", *Vehicle System Dynamics*, under review
6. Y. Xu, A. Kersten, S. Klacar, B. Ban, J. Hellsing, D. Sedarsky, "Improved efficiency with adaptive front and rear axle independently driven powertrain and disconnect functionality," *Transportation Engineering*, Vol. 13, 2023.
7. R.E. Bellman, S.E. Dreyfus, "Applied Dynamic Programming", Princeton University Press, Princeton, New Jersey, USA, ISBN 978-0-691-07913-4, 1962.
8. W. Leonhard, Control of Electrical Drives, Springer-Verlag, Berlin, 2001.